The effect of network formation on the mechanical properties of 1D:2D nano:nano composites

Cian Gabbett,[1] Conor S Boland,[1] Andrew Harvey,[1] Victor Vega-Mayoral,[1] Robert J Young,[2] Jonathan N Coleman[1]*

[1]*School of Physics, CRANN and AMBER Research Centres, Trinity College Dublin, Dublin 2, Ireland*

[2]*National Graphene Institute and School of Materials, The University of Manchester, Manchester, M13 9PL, United Kingdom*

*colemaj@tcd.ie

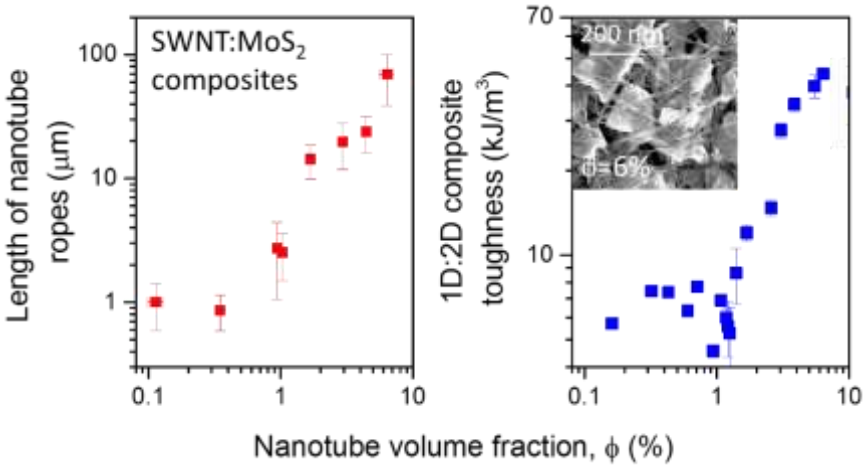

ToC fig

ABSTRACT: Mixtures of 1D carbon nanotubes and 2D nanosheets are important in electrochemical applications where the nanosheets are the active material, while the nanotubes provide electrical conductivity and mechanical reinforcement. While the conductivity of such nano:nano composites has been studied, the mechanical properties have not. Here we report a detailed study of the structural, electrical and mechanical properties of composites of MoS_2 nanosheets mixed with carbon nanotubes at various volume fractions, ϕ. Microscopic analysis reveals the nanotube network to evolve from a loosely connected structure for ϕ<1% to a strongly entangled continuous structure for ϕ>1%. Significantly, while the network consists of low (~200) aspect-ratio bundles for ϕ<1 vol%, above this value entangled ropes predominate, with the aspect ratio rising sharply with increasing ϕ, reaching ~4700 for the 6.4 vol% sample. While this transition does not affect the electrical properties, it has a significant effect on the mechanical properties. Below ϕ=1%, both the modulus and failure strain follow short-fibre composite behaviour with the modulus increasing as per the rule of mixtures and failure strain falling with ϕ. However, above ϕ=1%, both parameters increase with ϕ, consistent with continuous-fibre network behaviour. The tensile strength also transitions at 1 vol% from a regime limited by the matrix-fibre interfacial strength (ϕ<1 vol%) to one limited by the strength of the ropes (ϕ>1 vol%). Similarly, the toughness is constant at low volume fraction but increases strongly for ϕ> 1 vol%, consistent with a model based on percolation theory.

1. INTRODUCTION

Nanocomposites that consist of a matrix phase combined with a nanoscale filler material have been studied intensely for decades. Possibly the most well-studied nano-scale filler materials are carbon nanotubes[1, 2] and graphene nanosheets[3, 4] which, among other things, have been used to improve the electrical, thermal and mechanical properties of matrices. There are a number of classes of nanocomposite including polymer-matrix, ceramic-matrix and metal-matrix nanocomposites.[5] However, one property that these systems have in common is that the matrix is usually a continuous phase in which the filler particles are embedded. This paradigm has recently been disrupted by the rise of a new class of composite, which we refer to as the nano:nano composite.

Nano:nano composites are mixtures of two different nanomaterials, for example carbon nanotubes and 2D nanosheets,[6] and are fundamentally different to standard nanocomposites. Because both components are nano-structured and neither is continuous, the definition of matrix/filler is not predetermined by structural considerations. In addition, these composites are extremely porous which lends them to specific applications, for example in electrochemical devices where electrolyte can be introduced into the pore volume.[7] Such applications cast light on the attractiveness of nano:nano composites. As an example, while silicon nanoparticles have exceptionally-high theoretical lithium storage capabilities, their low electrical conductivity results in very poor performance for battery electrodes fabricated from nanoparticle films. However, the addition of small amounts of graphene has been shown to increase the electrode conductivity, thus dramatically increasing battery performance.[8] Thus, the role played by the materials can be used to define matrix and filler, with graphene playing the role of the filler in the previous example. This allows us to define subclasses of nano:nano composites in terms of the filler and matrix dimensionalities. For example, the graphene-silicon nanoparticle composite described above would be a 2D:0D nano:nano composite (or 2D:3D, depending on Si particle size). A large number of papers have appeared over the last few years reporting 2D:2D,[9-11] 1D:2D,[12-14] 2D:0D, [15, 16] 1D:0D[17, 18] and even 2D:1D:0D systems,[19] primarily for use in applications such as battery[12-14] or supercapacitor electrodes[20, 21] or photo/electro catalytic systems.[22, 23]

The most common fillers in nano:nano composites are nanotubes and graphene, whose primary role is to boost the conductivity of the matrix on order to facilitate charge distribution.[7, 24, 25] However, it has become apparent, that mechanical reinforcement is just as important as conductivity enhancement.[14] There are a number of reasons for this. In particulate-based films

poor mechanical properties make it impossible to fabricate arbitrarily thick electrodes from solution-processed nano-particles due to mechanical instabilities above a well-defined thickness known as the critical crack thickness (CCT).[26] Also, in battery and supercapacitor electrodes, repeated charge/discharge cycles can result in stress generation leading to electrode fragmentation, while bubble formation due to gas evolution in catalytic electrodes can also result in mechanical degradation.[27] While these problems can all be addressed by adding polymer binders, it has recently been shown that improved performance can be achieved at much lower additive levels using nano-fillers such as carbon nanotubes.[28]

However, while the mechanical advantages of nano-fillers in nano-matrices have been recognised,[7, 24, 25] virtually nothing has been done to characterise the mechanical properties of such systems. Very few papers have reported measurements of mechanical properties of nano:nano composites,[11, 14, 22] and none have engaged in mechanistic analysis. We address this gap here by performing detailed mechanical measurements and analysis on a model 1D:2D composite comprising carbon nanotubes in a matrix of MoS_2 nanosheets. We chose a 1D filler with the expectation that nanotube entanglement would lead to significant reinforcement while the matrix was selected due to the considerable potential for 2D materials in electrochemical applications.[29] We find considerable reinforcement with >10-fold increases in the composite stiffness, strength and toughness at loadings of <10 vol%. Most interestingly, we observe a structural transformation, leading to the development of a robust nanotube network at ~1 vol%. This leads to mechanical percolation, which has a significant impact on the composite mechanical properties.

2. RESULTS AND DISCUSSION

1D:2D nano:nano composites

The MoS_2 nanosheets were produced by liquid phase exfoliation[30, 31] in the solvent N-methyl-pyrrolidone (NMP) and were a few monolayers thick and had a mean lateral size of ~340 nm (figure 1A). The nanotubes (figure 1B) were sourced commercially and dispersed by sonication in dimethylformamide (DMF). Dispersions of nanosheets and nanotubes were mixed to give composite dispersions with a range of nanotube mass fractions ($M_f = M_{NT} / (M_{NT} + M_{NS})$) from 0 to 6 wt%. These dispersions were vacuum filtered to create free-standing films of thickness ~20-50 μm (figure 1C-D). Raman spectroscopic characterisation, measured on ~10 spots per sample spaced by >1 mm, clearly displays modes associated with both MoS_2 and SWNTs (figure 1E). The mean ratio of the MoS_2:SWNT mode

intensity scaled with $M_f^{-1}-1$, indicating that the composite contents were in line with expectation (figure 1F).[32] The MoS_2-only films were extremely brittle, frequently fragmenting on handling (figure 1G). However, the film stability increased markedly with nanotube addition, with composites containing >1 wt% nanotubes being extremely robust (figure 1H).

SEM analysis (figure 2 A-E) showed all films to consist of disordered arrays of nanosheets that are partially aligned in the plane of the film (figure 2A,C,D). As observed previously, such networks appear to contain significant porosity (figure 2D).[30] When imaging the surface of composite films, cracks were sometimes observed that were bridged[14, 33] by networks of one-dimensional objects formed from nanotubes aggregated into bundles or ropes (figure 2B). These bundles/ropes could also be observed protruding from film edges and fracture surfaces (figure 2E). In all cases, the nanotube-containing network appeared to be uniformly distributed and well mixed. More detailed analysis of SEM images will be presented below.

Structural and electrical properties

The filler volume fraction, ϕ, is an important parameter for the analysis of composite systems. These 1D:2D composites differ from more commonly studied systems, such as polymer-nanotube composites, in that they contain significant porosity as mentioned above. This means ϕ must be defined carefully, with the most natural definition being: $\phi = V_{NT} / V_{Film}$ where V_{NT} and V_{Film} are the total nanotube and total film volumes. The film volume can be more fully described by $V_{Film} = V_{NT} + V_{NS} + V_P$ with V_{NS} and V_P representing the total nanosheet and pore volumes respectively. Within this definition, the matrix consists of the nanosheets plus pores. The volume fraction can then be related very simply to the mass fraction as: $\phi = M_f \rho_{Film} / \rho_{NT}$. We measured the density of all films, finding values close to 2100 kg/m^3. This allowed us to calculate ϕ, which is plotted versus M_f in figure 3A. By considering the masses and volumes of the individual components, as well as the porosity $\phi_P = V_P / V_{film}$, we can find an expression for the film density which leads to a relationship between ϕ and M_f:

$$\phi = \frac{(1-\phi_P)}{1+\frac{\rho_{NT}}{\rho_{NS}}\frac{(1-M_f)}{M_f}} \qquad (1)$$

Fitting equation 1 to the data in figure 3A gives a mean film porosity of $\langle \phi_P \rangle$=56% (taking nanotube and nanosheet densities of ρ_{NT}=1400 kg/m^3 and ρ_{NS}=5060 kg/m^3). This porosity value is similar to values found for both solution-processed nanosheet-only[34] and nanotube-only[35] networks and is large enough to make these composites attractive for a number of applications, such as in electrochemical devices where electrolyte can be introduced into the considerable pore volume.[36] We note that, even though equation 1 fits the data in figure 3A reasonably well using a M_f-independent, mean porosity, this may mask small systematic porosity variations. To test this, we used equation 1 to calculate ϕ_P direct from the ϕ-M_f data. This data is plotted versus M_f in figure 3A, inset and shows a systematic variation, characterised by a well-defined minimum at ~1wt%. Although the details of this M_f-dependent porosity are not understood, this minimum will be mentioned again below.

We measured the in-plane electrical conductivity of all composite samples, finding an increase from ~10^{-5} S/m for MoS_2 to 8000 S/m for the highest loading sample (figure 3B). Such data are usually described using percolation theory, a framework where the conductivity increases only above the percolation threshold, $\phi_{c,e}$. This corresponds to the critical volume fraction where the first complete nanotube path spanning the sample appears. Above this threshold, the composite conductivity, σ_e, scales as:

$$\sigma_e = \sigma_{e,0}(\phi - \phi_{c,e})^{n_e} \qquad (2)$$

where $\sigma_{e,0}$ is related to the nanotube conductivity and n_e is the electrical percolation exponent. As shown in figure 3C, this equation fits the data well. Notably the percolation threshold is quite low ($\phi_{c,e}$=0.16%) while the exponent (n_e=2.1) is close to its universal value of 2.0.[37] In polymer-based composites, n_e is often[38] >>2 with the deviation attributed to a broad range of junction resistances due to the presence of polymer chains in the vicinity of nanotube-nanotube junctions.[39, 40] Here, the particulate nature of the MoS_2 matrix allows for intimate contact of nanotubes at junction sites, narrowing the range of junction resistances and leading to an exponent very close to its universal value.

For completeness we also measured the out-of-plane conductivity of the 5.8 vol% SWNT:MoS_2 composite, finding a value of ~1 S/m. This value (figure 3B, blue square) is far below the in-plane value, showing these composites to be highly anisotropic with the nanotubes predominately aligned in-plane. In addition, we measured the conductivity of a 5 wt% Graphene:MoS_2 composite, finding a very low value of ~10^{-4} S/m. This is consistent with the

fact that graphene-filled composites display much higher percolation thresholds than nanotube-filled composites.[32] The higher attainable conductivity of nanotube-filled over graphene-filled nano:nano composites is a substantial advantage, especially if significant in-plane alignment occurs.

Mechanical properties

While the electrical properties of 1D:2D composites have been reported,[32, 36] their mechanical properties remain almost completely unexplored. This is a significant gap because of the importance of mechanical robustness for the use of 1D:2D nanocomposites in applications such as battery electrodes.[14] We performed tensile tests on a number of composite strips (figure 4A) for each volume fraction. In addition, we measured the mechanical properties of SWNT-only films (often referred to as Buckypaper) for comparison. Tensile stress-strain curves were measured for a range of films with a subset of curves shown in figure 4B (see SI for a discussion of the difficulties associated with such measurements). We found the MoS_2-only sample to be so fragile that it was impossible to get reliable mechanical data from it. The composite stress-strain curves were slightly sublinear with a clear increase in stress at all strains as nanotube content is increased. From the curves, it is possible to extract the composite elastic modulus, E_c, tensile strength, σ_c, strain-at-break, ε_c, and tensile toughness, T_c (equal to the area under the stress-strain curve and equivalent to the energy absorbed up to fracture). These data are plotted as a function of nanotube volume fraction in figures 4C-F. In the next few paragraphs we will describe the data qualitatively with detailed analysis coming later in the paper.

The extracted Young's moduli are plotted versus ϕ in figure 4C. This plot shows a near-linear increase in E_c up to ϕ~1%, after which E_c appears to fall slightly before then increasing again, reaching ~1 GPa for the 9.4 vol% composite with the value for the SWNT-only film appearing to be in line with this trend. Shown in figure 4D is a graph of composite strength plotted versus ϕ. The lowest loading level composite (ϕ=0.16 vol%) was extremely weak with a strength of ~0.5 MPa. However, on the addition of nanotubes the strength increased continuously, reaching ~5.5 MPa for the 9.4 vol% sample. Although this maximum strength is well below the SWNT-only value of ~35 MPa, this >10-fold increase in strength transforms the material from being too brittle to handle to being mechanically robust, resembling a thermoplastic. Interestingly, we found the strength to scale sublinearly with ϕ as a well-defined power law with exponent close to 1/2. This is in contrast to most reported polymer-nanotube

composites, which tend to display a linear increase of strength with ϕ, at least at low volume fraction.[41] The strain-at-break, ε_c, is plotted versus ϕ in figure 4E. Here we see a well-defined fall-off in ε_c with nanotube content, from ε_c ~2% at low ϕ, reaching a minimum of ε_c ~0.5% at ϕ=1 vol%. Above this volume fraction ε_c rises again, reaching ε_c ~2% at ϕ=4-8 vol%. Interestingly, the breaking strain appears to fall off at higher values of ϕ, leading to a value of ~1% for the SWNT-only films. Finally, the tensile toughness is plotted versus ϕ in figure 4F. This parameter was initially ~5 kJ/m^3, roughly invariant with nanotube loading up to ~1 vol%. However, above ϕ=1 vol% the toughness increases sharply, reaching ~45 kJ/m^3 for the 6.4 vol% sample. Again, the toughness-value measured for the SWNT-only sample was in line with this trend. We note that the toughness is particularly important from an applications standpoint, with a recent report linking increased toughness with enhanced stability in 1D:2D battery electrodes.[14]

For comparison purposes, we measured the mechanical properties of a 2D:2D nanocomposite, fabricated by mixing nanosheets of MoS_2 and graphene (5 wt%). This was performed using methods almost identical to those used to prepare the SWNT:MoS_2 composites. The values are plotted in figure 4C-F as black stars. While the measured modulus of the Graphene:MoS_2 composite was similar to that of the SWNT:MoS_2 composites of equivalent ϕ, the strength, failure strain and toughness were all much lower for the 2D:2D composite compared to the 2D:1D composites. We believe this is a geometric effect linked to the fact that while nanotubes can entangle, graphene nanosheets cannot.

We have also compared these results to literature data for the mechanical properties of similar materials, namely nanotube paper, graphene paper and nano-cellulose-graphene composites (see SI). We find the mechanical properties of our NT-only material to be consistent with published NT-Buckypapers but somewhat inferior to both graphene paper and other nano:nano composites such as nano-cellulose/graphene hybrids. In the latter case the superior mechanical properties are almost certainly linked to the strong hydrogen bonding found in nano-cellulose-based systems.

It is clear from figure 4 that the data for the modulus, strain-at-break and toughness all display a discontinuity at ϕ~1% (the strength data contains a less obvious discontinuity at ~1 vol%) which is reminiscent of the porosity minimum observed in figure 3A. For the modulus data, the maximum in E_c, that occurs here around 1 vol%, is usually taken to imply that the aggregation state of the nanotubes changes at this volume fraction. In addition, the changes in

both the ε_c and T_c behaviour at ϕ=1 vol% are consistent with a changeover of fracture mechanism at this loading level. To understand the nature of this change, it will be necessary to examine the morphology of these composites.

Network morphology

To investigate the mechanism of the change in mechanical properties at ϕ=1 vol%, we performed an extensive SEM characterisation of the planar and fracture surfaces for composites with a range of nanotube loading levels. Shown in figure 5A-F are representative images for both low (<1 vol%, top row, A, C, E) and high (>1 vol%, bottom row, B, D, F) nanotube loading levels. These images are separated into those collected from planar surfaces (A-B), fracture surfaces (C-D), and images of surface cracks (E-F), which afford a limited view of the composite interior in a state which is not influenced by fracture. In all cases, these images show similar trends. At the lowest loading levels (figure 5 A, C, E) the images show relatively small numbers of isolated 1D objects, which we assume to be small bundles (individual nanotubes are rarely found in liquid exfoliated samples produced without ultracentrifugation unless the concentration is very low).[42] However, for the higher loading level samples (figure 5 B, D, F), all bundles appear to belong to a dense network that extends throughout the sample. This high-ϕ network appears to consist of one-dimensional objects that are somewhat thicker than those observed for ϕ<1 vol%. In addition, while it is impossible to assess the length of the one-dimensional objects directly from the SEM images, those in the ϕ>1 vol% composites appear much longer than those in low nanotube-content composites.

In order to understand this transition from individual bundles to a collective network of fibres it is necessary to know how the dimensions (diameter, D_F, and length, L_F) of the one-dimensional objects observed in SEM scale with ϕ. The 1D fibre diameter can be readily measured from SEM images (see SI for histograms) with the resultant means plotted versus ϕ in the inset of figure 5G. Here we find the bundle diameter to be constant at D_F≈5 nm for ϕ<1%. However, above 1 vol%, we see a smooth increase, reaching D_F=15 nm for ϕ=6.4 vol%. This implies that above 1 vol%, nanotube aggregation becomes important. We found it impossible to directly measure the length of the one-dimensional fibres because very few were found with both ends visible in a single image. However, it was possible to indirectly measure the length of the 1D fibres by noting that the number of fibre ends per unit area is given by: $N_{Ends} / A = 2N_F / A$, where N_F / A is the number of 1D fibres per unit area. In addition, the

total length of all 1D fibres contained in a given area is given by: $L_{\mathrm{F,T}} / A = L_F \times N_{\mathrm{F}} / A$, where L_F is the mean length of the 1D fibres. Combining these definitions gives: $L_F = 2(L_{\mathrm{F,T}} / A) / (N_{Ends} / A)$. Crucially, both $L_{\mathrm{F,T}} / A$ and N_{Ends} / A can be measured from SEM images (see SI), leading to an estimate of the mean fibre length, L_F. Shown in figure 5G is a plot of the length of the 1D fibres as a function of ϕ. At low values of ϕ, L_F~1 μm, a value typical of small bundles of nanotubes. However, for ϕ>1 vol%, L_F increases sharply, reaching ~70 μm for ϕ=6.4 vol%. This dramatic increase in length, coupled with the slight diameter increase means that the aspect ratio (L_F/D_F) of the 1D objects changes dramatically from ~200 for ϕ<1 vol% to ~4700 for the 6.4 vol% sample. This change would be expected to have significant mechanical implications.

We believe these data can be explained as follows. At volume fractions below the electrical percolation threshold ($\phi_{c,e}$=0.16%), the nanotube bundles are either isolated or exist in small network fragments. It is only when the volume fraction reaches $\phi_{c,e}$ that the network of nanotube bundles first spans the sample, allowing current to flow. However, while networks just above $\phi_{c,e}$ are conducting, it is thought that they are not mechanically robust, largely because the average number of inter-bundle junctions is too low. For example, while two junctions per bundle is the minimum required to transfer charge, ~4 are required to yield mechanical stability of the nanotube network as a whole.[43] Thus, there is a range of volume fractions, just above $\phi_{c,e}$, where the nanotube network requires the presence of the matrix to ensure its stability. In this ϕ-range the nanotube network is effectively embedded in the matrix, and behaves similarly to a polymer- or ceramic-matrix composite. However, in nanocomposites such as these 1D:2D composites, where the matrix is mechanically very weak and so cannot retard reorganisation of the filler during film formation, we expect new behaviours to emerge as the volume fraction is increased further. We propose that a critical value of ϕ exists where the nanotube network transforms from a poorly interconnected "weak" state to a heavily interconnected state that is mechanically robust. This "strong" network will consist of extremely long ropes comprised of entwined bundles. Such a transition is schematically depicted in figure 5H. We would expect these ropes to be strongly entangled, with the overall network resembling a nanotube Buckypaper, but with larger inter-rope pores that are occupied by nanosheets (and free volume). In such a system, we would not expect to be able to identify individual nanotube bundles due to their near complete integration into the rope network. We denote the critical ϕ-value, where the network transitions from weak to strong, as the

mechanical percolation threshold, $\phi_{c,m}$, and propose that, for $\phi \geq \phi_{c,m}$, all mechanical properties of the system are essentially those of the nanotube network with minimal contribution from the matrix. The data in figure 5G would imply that $\phi_{c,m}$~1 vol%. Interestingly, $\phi_{c,m}$ is close to the nanotube loading level associated with the porosity minimum shown in the inset of figure 3, providing further evidence of the morphological basis of this transition.

It is interesting to note that electrical conductivity data (figure 3B-C) appears to be completely un-perturbed by the morphological transition which occurs at $\phi_{c,m}$. This implies that, although the transition from a short-fibre composite-like structure to a network-like structure has significant mechanical implications, it hardly affects the current-carrying capability of the network.

It is difficult to image the transition directly from a weak to strong network because the presence of nanosheets (~95-99.9% by mass) tends to obscure the nanotube network structure. However, we note that a similar process has been observed by other groups. For example, Song et al.[44] performed experiments building up SWNT-only films by successive dip coating. Their published SEM images clearly show that after 100 dips, the network is weak, consisting of criss-crossed bundles whose individual character is clearly visible. That is, individual bundles contributing to the network can be seen and many bundle ends are observable. However, after 400 dips, the network noticeably changed in character: the network now consists of much thicker objects which are ropes of entwined bundles. These ropes display Y-shaped bifurcations that act like inter-rope junctions but would be expected to be much more robust. In addition, the network appears to be continuous: it is impossible to identify individual bundles and no ends can be seen. We believe these characteristics also apply to the SWNT network in 1D:2D nano:nano composites.

Modelling mechanical properties

With this transition between weak and strong networks in mind, we can develop simple yet quantitative models to describe the mechanical properties of 1D:2D nano:nano composites such as these.

Modulus: At low loading, we expect the composite to consist of a sparse network of weakly interacting small bundles in a matrix of MoS_2 nanosheets. Assuming that some stress can be transferred across the nanosheet/nanotube interface, the modulus of such a composite, E_c, can be described by the rule of mixtures incorporating shear lag theory:[5]

$$E_c = \eta_o \eta_L E_F \phi + E_M (1-\phi) \quad (3a)$$

where η_o is the filler orientation efficiency factor, η_L is the filler length efficiency factor, E_F is the filler modulus and E_M is the matrix modulus. Within the framework of shear lag theory, η_L is given by:[5]

$$\eta_L = 1 - \frac{\tanh(nL_F / D_F)}{nL_F / D_F} \quad (3b)$$

where L_F and D_F are the filler length and diameter while:

$$n = \left[\frac{2E_M}{E_F(1+\nu_M)\ln(1/\phi)} \right]^{1/2} \quad (3c)$$

where ν_M is the Poisson ratio of the matrix.

Assuming $E_M << E_F$, we follow the method of Young et al.[45] by Taylor-expanding the hyperbolic tangent and combining equations 3a, 3b and 3c to give:

$$E_c = E_M \left(1 - \phi + \frac{2L_F^2}{3D_F^2} \frac{\eta_o}{(1+\nu_M)} \frac{\phi}{\ln(1/\phi)} \right) \quad (4)$$

This equation is expected to apply well to composites with low modulus matrices[45] and, as can be seen in figure 4C, fits the data extremely well for ϕ<1%. Taking ν_M=0.5 and η_o=3/8 (appropriate when the fillers are aligned in-plane[46]), the fit yields L_F/D_F=175±30, a value which is in line with the data in figure 5G. In addition, this fit gives a matrix modulus of ~16 MPa, reasonably close to the previously reported stiffness of MoS_2 nanosheet networks (26±7 MPa).[14]

However, this model clearly does not apply for ϕ>1% where we expect the nanotubes to form into an entangled network that can bear load independent of the matrix. The original version of shear-lag theory was designed to describe just such a system[47] and is now widely used to model bonded-fibre networks such as those found in paper. Provided a fibre network is dense enough, the modulus can be modelled using (see SI):[48]

$$E_c = \eta_o E_F (\phi - \phi_{c,m}) \quad (5)$$

where $\phi_{c,m}$ is a constant which can be thought of as the mechanical percolation threshold. In figure 4C, we have fitted equation 5 to the data for ϕ>2 vol% (fixing $\phi_{c,m}$=1.2 vol% and taking

η_o=3/8). This gives a good match to the data for E_F=29±4 GPa. Interestingly, the SWNT-only data point sits close to this line, as would be expected for a model describing fibre networks. We note that this theory is thought to somewhat underestimate the true fibre modulus,[48] and indeed this modulus value is considerably smaller than the value of ~100 GPa reported for bundles/ropes with diameter ~10-15 nm.[49]

Strength: While the strength data shown in figure 4D display a slight discontinuity around ϕ=1%, what is just as unusual is its well-defined sublinear dependence on ϕ. Usually continuous matrix nanocomposites show either a linear increase of strength with filler content (if the filler is well dispersed) or a decrease in strength with loading (if the filler is poorly dispersed).[41] The strength of fibre networks is usually described by models such as that of Page.[50] However, the Page equation implies a near-linear relationship between strength and fibre volume fraction (see SI) and so is inconsistent with our data.

After a comprehensive search of the literature, we found a family of models that predict a sub-linear σ_c-ϕ relationship for fibre-reinforced composites.[51-53] Such models assume failure can occur via three distinct processes, each dominating for a range of angles (θ) between the fibre and the applied stress. These are fibre failure (low-θ), interfacial shear failure (intermediate-θ) and transverse matrix failure (i.e. in a plane parallel to a fibre axis, that occurs at high-θ). However, published models incorporate all three failure processes and do not provide a good fit to our data. We found that by considering only two failure mechanisms, we could obtain an equation that described the experimental data very well (see SI). We modified the approach of Lees at al.[51-53] to consider only fibre breakage and transverse matrix failure, reasoning that shear failure could be introduced in an alternative manner (see below). The remaining two processes are associated with failure stresses of $\sigma_{FB} = \sigma_{\parallel} / \cos^2\theta$ and $\sigma_{TF} = \sigma_{\perp} / \sin^2\theta$ respectively. Here $\sigma_{\parallel}$ represents the strength of a composite containing only fibres aligned parallel with the direction of applied stress and $\sigma_{\perp}$ is the strength of that composite in the transverse direction (perpendicular to the fibres).[51],The composite strength can then be found by taking average of these stresses over the appropriate θ-range (see SI) to give:

$$\sigma_c = 4\sqrt{\sigma_{\parallel}\sigma_{\perp}} / \pi \,. \qquad (6a)$$

We can make the approximation that $\sigma_{\perp} \approx \sigma_M$, the matrix strength, while $\sigma_{\parallel}$ can be found from the rule of mixtures. For an aligned fibre composite the rule of mixtures states that the strength is given by:[46]

$$\sigma_{\parallel} = \eta_{L,S}\sigma_F\phi + (1-\phi)\sigma_M \quad (6b)$$

Here σ_F is the fibre (in this case a nanotube bundle) strength while $\eta_{L,S}$ is the strength efficiency factor. The efficiency factor takes one of two values, depending on whether the fibre length is above or below a critical value, L_c. This value is given by:[5] $L_c = \sigma_F D_F / 2\tau_{MF}$ where D_F is the fibre diameter and τ_{MF} is the shear strength of the matrix-fibre interface. For $L_F<L_c$, $\eta_{L,S} = L_F / 2L_c$ while for $L_F>L_c$, $\eta_{L,S} = 1 - L_c / 2L_F$.[46] According to figure 5G, when ϕ<1 vol%, the fibres comprising the network are bundles of length ~1 μm. This length is close to the typical length of individual SWNT which means the constituent nanotubes probably span the full bundle length. This implies that, when ϕ<1 vol%, the bundles are extremely strong, having a strength close to the individual nanotube strength. As a result, the critical length should be extremely high and we expect $L_F<L_c$. However, for ϕ>1%, the fibres consist of very long ropes of entwined bundles. As a result of their length, and because such ropes should have lower strength compared to individual nanotubes,[54, 55] we expect $L_F>>L_c$ in this range, allowing us to approximate $\eta_{L,S} \approx 1$ when ϕ>1%. Then, combining equations 6a and 6b with the efficiency factors gives:

$$\sigma_c(L_F < L_c) = \frac{4}{\pi}\left[\sigma_M \tau_{MF} \frac{L_F}{D_F}\phi + \sigma_M^2(1-\phi)\right]^{1/2} \quad (6c)$$

$$\sigma_c(L_F > L_c) \approx \frac{4}{\pi}\left[\sigma_M \sigma_F \phi + \sigma_M^2(1-\phi)\right]^{1/2} \quad (6d)$$

We note that equation 6c now incorporates interfacial failure via τ_{MF}. We have used these expressions (equation 6c for ϕ<1.2 vol% and equation 6d for ϕ<1.2 vol%) to fit the data in figure 4D. Both cases are consistent with $\sigma_M = 0.14 \pm 0.05$ MPa, while the first equation yields τ_{MF}=4.1±0.2 MPa (taking L_F/D_F=200 from the SEM data in figure 5G). The former value is reasonably consistent with previous work which measured the strength of MoS_2 networks to be 0.24±0.06 MPa.[14] While τ_{MF} is within the reported range for filler-matrix interfacial shear strengths,[56] it is considerably smaller than values of 20-60 MPa usually found for polymer–

nanotube composites.[56] Thus, it should be emphasised that values of τ_{MF}~4 MPa would imply the interfaces between matrix and filler to be relatively weak. This is as-expected for a discontinuous matrix which should display less intimate contact with the bundle surfaces compared to polymer-nanotube composites.[57, 58]

Fitting the data above 1 vol%, we find σ_F=1.2±0.1 GPa, a value which is consistent with literature reports that show SWNT bundles to have strengths of a few GPa.[54, 55] Combining these fibre strength and shear strength values shows that the ropes found in the composites for ϕ>1 vol% have critical aspect ratios of ~200. With reference to the data in figure 5G, this means that composite failure will begin to occur via fibre failure once the volume fraction exceeds 1%, where ropes form and L_F/D_F surpasses 200.

We can test the credibility of this value for bundle strength by using it to estimate the inter-nanotube interfacial shear strength, τ_{NT}. We loosely follow the methodology of Vilatela et al.,[59] making slight modifications. Failure of a nanotube bundle or rope tends to be via pullout of the nanotubes from their sockets. The force required to pull out each nanotube is the interfacial shear strength, τ_{NT}, times the pullout area: $F_1 = \tau_{NT} \times (\pi D_{NT} / 2) \times L_{NT} / 4$, where D_{NT} is the nanotube diameter and L_{NT} is the nanotube length. The factor of 2 comes from the fact that, on average, half the nearest neighbours of a given nanotube are attached to the same side of the fracture surface and so are stationary relative to it. The factor of four comes from the fact that the embedded length which is pulled out can vary between zero and $L_{NT}/2$ and so has a mean of $L_{NT}/4$. The bundle or fibre strength is the total force due to all nanotubes intersecting the fracture surface divided by the cross sectional area:

$$\sigma_F = \frac{F_1 \times (D_F / D_{NT})^2 / 2}{\pi D_F^2 / 4} = \frac{\tau_{NT} L_{NT}}{4 D_{NT}} \qquad (6e)$$

where D_F is the bundle diameter and $(D_F / D_{NT})^2$ represents the number of nanotubes intersecting the fracture surface. The factor of 2 in equation 6e is in addition to the one described above and is required to avoid double counting. Taking σ_F=1.2 GPa, D_{NT}~1 nm and L_{NT}~ 1 μm yields τ_{NT}~4.8 MPa. This value is reasonable and agrees with the results of Vilatela's literature review which finds interfacial shear strengths in graphitic systems to cover a broad range centred on ~5 MPa.[59]

The data in figure 4C and 4D imply fibre moduli and strengths of 29 GPa and 1.2 GPa respectively. Assuming the bundle stress-strain response to be roughly linear, this implies the

bundle breaking strain to be ~4.5%. This is reasonably in line with the data in fig 4E which shows the composite breaking strain (due to bundles with a range of orientations) to be <2%. This implies the fibre modulus and strength values extracted from the models are broadly self-consistent but suggests the fibre modulus to be somewhat underestimated as described above.

Strain-at-break: The data for strain-at-break as a function of ϕ shown in figure 4E is very interesting and offers strong evidence for a change in the nanotube network structure at ϕ~1%. While it is difficult to develop quantitative models for breaking strain in composites, some points can be made. In the low-ϕ regime, where we expect the nanotube network to be weak, we see a clear fall-off in breaking strain with ϕ. Such behaviour is typical of polymer-nanotube composites.[41] This can occur for a number of reasons. For example, the presence of stiff filler particles can significantly constrain the matrix and reduce its ability to deform,[5] a factor that is particularly apparent for soft matrices.[60] The increasing breaking strain observed above ~1 vol% is extremely unusual in composites. However, such behaviour is common in networks of 1-dimensional fibres. A study of paper (i.e. a network of cellulose fibres) densified under different pressures has shown the most dense (highest fibre volume fraction) networks to have the highest breaking strain.[61, 62] This is a general phenomenon and has been linked to the increase in the overall inter-fibre bonded area with volume fraction.[62] Taken together, this interpretation of the strain-at-break data strongly supports the idea of a transition between weak networks resembling filler-matrix composites at low-ϕ to strong, continuous networks resembling fibre networks at high-ϕ.

Toughness: By definition, the tensile toughness is the work done per unit volume in stretching the sample to breaking point. Most of this work goes into increasing the elastic potential energy of the stretched sample. For brittle materials most of this energy is recoverable, although for real materials some plastic deformation will occur, for example by irreversible nanotube re-orientation. In addition, for a viscoelastic material, some of the elastic energy will be dissipated. Upon fracture, a portion of the elastic energy is used to create the fracture surface. This allows us to relate the work of fracture per unit area, W/A, to the toughness via the gauge length, L_0: $W/A = f(\phi, L_0) T_c L_0$, where $f(\phi, L_0)$ is the fraction of elastic energy which goes into creating the fracture surface. We would expect f to depend on ϕ and L_0 as well as other factors such as the structural properties of the composite.

As shown in figure 4F, the toughness is relatively constant for ϕ<1%. This is interesting as it implies that any increase in W/A associated with increasing the nanotube content for ϕ<1% is

balanced by changes in *f*. However, for ϕ>1% the toughness increases rapidly with nanotube content, implying that *W*/*A* then increases much faster than *f*. From SEM images such as those shown in figure 5D, it is clear that composite failure occurs via failure of nanotube ropes. The most likely failure mechanism is by nanotubes within ropes pulling out of their sockets[33] in a manner similar to the model reported by Vilatela et al. for nanotube fibres.[59] Here (and in the SI) we develop a model for the work of fracture under such circumstances, approximately following the method of Wagner et al. (but ignoring the hollow nature of the nanotubes).[63] This involves calculating the total energy associated with the frictional sliding of nanotubes out of their sockets. We find (see SI) that the work of fracture for nanotubes pulling out from a single bundle is given by:

$$W_{Bun} = \frac{\pi D_F^2 L_{NT}^2 \tau_{NT}}{96 D_{NT}} \left[1 - \frac{D_{NT}}{D_F} \left(1 - \frac{\tau_{MF}}{\tau_{NT}} \right) \right] \qquad (7a)$$

where τ_{MF} and τ_{NT} are the shear stresses at the matrix-nanotube (i.e. bundle edge) and nanotube-nanotube (i.e. bundle interior) interfaces. Normally, the total work of fracture for the composite would be found by multiplying this quantity by the number of bundles crossing the fracture surface (*N*/*A*). However, close to the mechanical percolation threshold, not all of these bundles will be fully connected to global nanotube network. We propose that these unconnected bundles do not fully contribute to the work of fracture and should be neglected. This means the overall work of fracture is given by:

$$\left(\frac{W}{A} \right)_{Net} = P(\phi) \left(\frac{N}{A} \right) W_{Bun} \qquad (7b)$$

where $P(\phi)$ is the fraction of those bundles connected to the main network. In percolation theory, $P(\phi)$ is known as the percolation probability and scales from $P(\phi)$=0 at low ϕ to $P(\phi)$=1 at ϕ=1. Taking $N / A = 4\phi / \pi D_F^2$ (see SI) yields:

$$\left(\frac{W}{A} \right)_{Net} = P(\phi)\phi \frac{L_{NT}^2 \tau_{NT}}{24 D_{NT}} \left[1 - \frac{D_{NT}}{D_F} \left(1 - \frac{\tau_{MF}}{\tau_{NT}} \right) \right] \qquad (7c)$$

For 1D:2D composites, we found above that $\tau_{MF} \sim \tau_{NT}$, while in general $D_{NT} << D_F$, allowing us to make the approximation:

$$\left(\frac{W}{A}\right)_{Net} \approx P(\phi)\phi\frac{L_{NT}^2\tau_{NT}}{24D_{NT}} \quad (7d)$$

Within percolation theory, there is no analytical expression for $P(\phi)$. However, we assume it can approximately be written in the form: $P(\phi)=\left(\frac{\phi-\phi_{c,m}}{1-\phi_{c,m}}\right)^k$, where k can be considered to be the mechanical percolation exponent. This form fulfils the criteria laid out above and allows us to write:

$$T_c \approx \frac{\phi}{f(\phi,L_0)}\left(\frac{\phi-\phi_{c,m}}{1-\phi_{c,m}}\right)^k\frac{L_{NT}^2\tau_{NT}}{24D_{NT}L_0} \quad (7e)$$

By fitting the T_c vs ϕ data for 1%<ϕ<6.4%, we have found that $T_c \propto (\phi-\phi_{c,m})^k$, which implies that $f(\phi,L_0)=C\phi$ where C is a dimensionless constant (at least over the examined ϕ-range). This means that:

$$T_c \approx \frac{1}{C}\left(\frac{\phi-\phi_{c,m}}{1-\phi_{c,m}}\right)^k\frac{L_{NT}^2\tau_{NT}}{24D_{NT}L_0} \quad (7f)$$

Using this function, we have fitted the data in figure 4F for ϕ>1 vol% (black line). We find an extremely good fit which gives k=0.47, $\phi_{c,m}$=1.2% and, taking D_{NT}~1 nm and L_{NT}~ 1 μm, yields τ_{NT}/C=21.6 MPa. Interestingly, the SWNT-only data point sits close to this line as would be expected for a model describing fibre networks. If we assume τ_{NT} is similar to the interfacial shear strength estimated above using the strength data, we can estimate C~0.22. This implies that at ϕ=10%, for example, only ~2.2% of the stored elastic energy is converted to work of fracture.

This toughness data, combined with the model described above are particularly interesting. This data clearly exhibits percolation-like behaviour and, unlike the modulus and strength data, shows a sharp increase with nanotube content only once the volume fraction exceeds $\phi_{c,m}$=1.2%. This is important because in some applications, such as the stabilisation of battery electrodes,[14] tensile toughness is the key parameter. This data clearly shows that meaningful increases in toughness cannot be achieved until the percolation threshold is surpassed.

3. CONCLUSIONS

In conclusion, we have performed a detailed mechanical analysis on composites of liquid exfoliated nanosheets mixed with carbon nanotubes. Such composites consist of interpenetrating disordered networks of nanosheets and nanotubes and display a porosity of ~56%, independent of nanotube content. For nanotube volume factions below 1%, the nanotube network is comprised of small bundles with aspect ratios of ~200. However, above this volume fraction, the network undergoes a transformation to a more continuous network dominated by extremely long ropes with aspect ratios of up to 4700. This transition has a significant effect on the mechanical properties. Below 1 vol%, the modulus, strength, breaking strain and toughness behave in a manner similar to that observed for polymer-nanotube composites. However, above 1 vol%, the behaviour shifts to resemble that of a fibrous network. In general adding nanotubes yields significant increases in mechanical properties. Compared to the nanosheet matrix, addition of 5 wt% nanotubes leads to increases in modulus, strength and toughness by ×55, ×70 and ×10 respectively. These increases transform the properties of the material, rendering it robust and suitable for a range of applications.

4. MATERIALS AND METHODS

Materials

Molybdenum(IV) sulfide powder (MoS_2, 99%, CAS 1317-33-5) and dimethylformamide (DMF, CHROMASOLV Plus, ≥ 99.9%) were obtained from Sigma-Aldrich (Dublin, Ireland). 1-methyl-2-pyrrolidinone (NMP, CHROMASOLV Plus, ≥ 99%) was purchased from Honeywell Riedel-de Haën. P3-SWNT (CNT, > 90%, contains 1.0–3.0 atomic % carboxylic acid groups, which can be derivatized with a variety of functional groups) were obtained from Carbon Solutions Inc. Polyester track-etched membranes (PETE, pore size 0.1 μm, 47 mm diameter) were purchased from Sterlitech. Whatman Anodisc 47 alumina membranes (pore size 0.02 μm, 47 mm diameter) were purchased from GE Healthcare. Holey carbon grids (400 mesh) were purchased from Agar Scientific (U.K).

Preparation of MoS_2 Stock Dispersion

As part of an initial cleaning step, eight grams of MoS_2 in 80 ml of NMP was sonicated for 1 hour using a horn-probe tip sonicator (Sonics Vibra-cell VCX-750W ultrasonic processor) operating at 60 % amplitude. The dispersion was processed in a 100 ml stainless steel beaker under ice cooling with the tip pulsed at 4 s on and 4 s off to avoid damage to the processor and

overheating of the solvent. The resulting dispersion was then placed into three 28 ml glass vials and centrifuged for 60 minutes at 4900 RPM (240 g Hettich Mikro 220R, fixed angle rotor) to isolate the purified MoS_2 in the sediment. The supernatant was discarded and the sediment was redispersed in 80 ml of NMP and sonicated for a further 6 hours (60 % amplitude, pulsed at 4 s on and 4 s off). The resulting dispersion was then centrifuged for 1 hour at 1000 RPM to remove unexfoliated material. The sediment was reused for further exfoliation. The dispersion supernatant was decanted and centrifuged for a further 2 hours at 4900 RPM. The NMP supernatant was then decanted and the MoS_2 sediment in each vial was redispersed in 10 ml of DMF using an ultrasonic bath (Thermo Fisher Scientific, FB11201, 37 kHz).

Preparation of SWNT:MoS_2 Stock Composites

Twenty milligrams of P3-SWNTs were added to 20 ml of DMF at a concentration of 1 mg/ml. The dispersion was sonicated for 2 hours in a tapered-probe sonic tip (25 % amplitude, 750 W ultrasonic processor) pulsed at a 6-2 on/off ratio. As both the MoS_2 and SWNTs were dispersed in the same solvent, we could readily mix the dispersions to form composite dispersions of any desired ratio. The concentration of the MoS_2 dispersion was determined by filtration onto an alumina membrane and weighing. By directly mixing the SWNT dispersion with a predetermined concentration of MoS_2 dispersion, a series of SWNT:MoS_2 composites with SWNT content ranging from 0 - 6 wt% were formed.

Characterisation

High resolution images of the prepared SWNT:MoS_2 composites were obtained using a Zeiss Ultra Plus scanning electron microscope. An accelerating voltage of 2-3 kV, with a 30 μm aperture at a working distance of 3-5 mm was used. Bright-field transmission electron microscopy was performed using a JOEL JEM-2100 LaB6 TEM operated at 200 kV. The samples used in the TEM measurements were dispersed in 2-propanol and dropped onto holey carbon grids on a filter membrane to absorb the excess solvent. Statistical analysis of the TEM-measured flake dimensions was performed by measuring the longest axis of each nanosheet and assigning it as the length, followed by a measurement along the axis perpendicular and assigning it as the width. Raman measurements were performed using a Horiba LabRam HR800 spectrometer. The 632.8 nm excitation wavelength was used with a laser power below 0.2 mW on a spot size of 1.5 μm. The signal was collected using a 100× objective lens (0.8 numerical aperture) and a 600 grooves per millimetre grating was used in order to achieve a spectral resolution of approximately 1.2 cm^{-1}. Measurements were performed at room temperature and no degradation or heating effects were observed at the chosen laser fluence.

Each spectrum is the average of 4 measurements with the signal acquisition time being 30 seconds for samples having a SWNT loading of ≥ 0.6 wt% and 120 seconds for all others. The standard deviation was calculated by measuring a minimum of 20 spectra in random positions along the sample, for each sample.

Film Formation and Electrical and Mechanical Measurements

Composite dispersions were vacuum filtered onto PETE membranes and dried overnight at room temperature. The free-standing composite films were then peeled off and cut into strips 2.5 mm wide. Film thicknesses in the range 20-50 μm were measured using a digital micrometer. Because of their extremely poor mechanical properties, the very low mass fraction films were produced with higher thicknesses to increase the breaking forces. Mechanical measurements were recorded using a Zwick-Roell tensile tester (Xforce P, 100 N load cell) at a strain rate of 0.5 mm/min. Electrical conductivity values were calculated from resistance measurements using the four-point probe technique with a source meter (Keithley 2400, Keithley Instruments Inc.). Each mechanical and electrical data point is the average of 4 measurements. The films were also used for Raman spectroscopy and scanning electron microscopy.

ACKNOWLEDGEMENTS

We acknowledge financial support from the SFI-funded AMBER research centre (SFI/12/RC/2278). JNC and RJY acknowledge funding from the European Union Seventh Framework Programme under grant agreements n°604391 and n°696656 Graphene Flagship.

ASSOCIATED CONTENT

Supplemental Information

Short gauge length effects, detailed derivations, detailed description of microscopy results and literature comparison. This material is available free of charge via the Internet at http://pubs.acs.org.

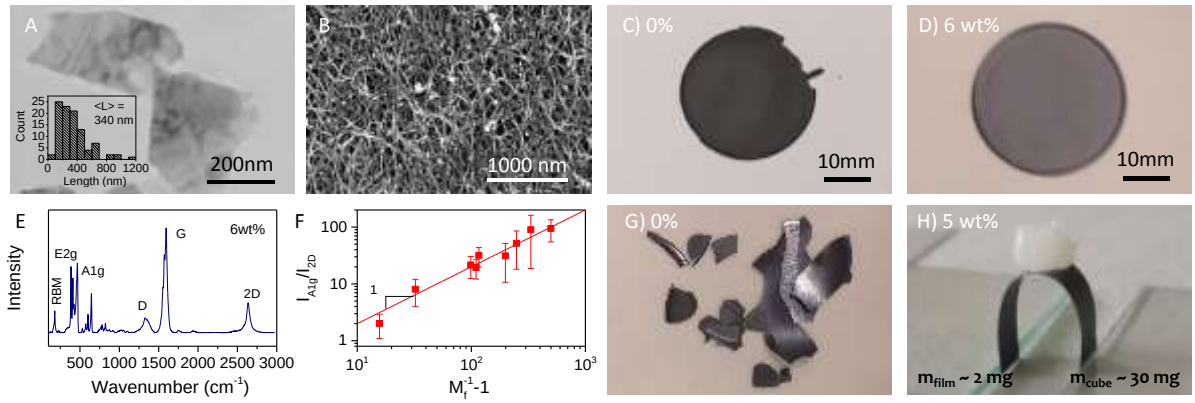

Figure 1: (A) Representative TEM image of liquid exfoliated MoS_2 nanosheets. Inset: Lateral size distribution. (B) SEM image of a vacuum filtered network of SWNTs. (C-D) Photographs of vacuum filtered films of (C) MoS_2 (~50 μm thick) and (D) SWNT:MoS_2 (6 wt%, ~20 μm thick). (E) Typical Raman spectrum of a 6 wt% composite showing modes associated with both MoS_2 (E_{2g} and A_{1g}) and SWNTs (RBM, D, G and 2D). (F) Intensity ratio of A_{1g} to 2D modes showing linearity when plotted versus $M_f^{-1} - 1$, indicating the composition is as expected. (G-H) Visual representations of the brittleness of MoS_2-only networks – this one fragmented on handling (G) – and the robustness of a 5 wt% composite network (H).

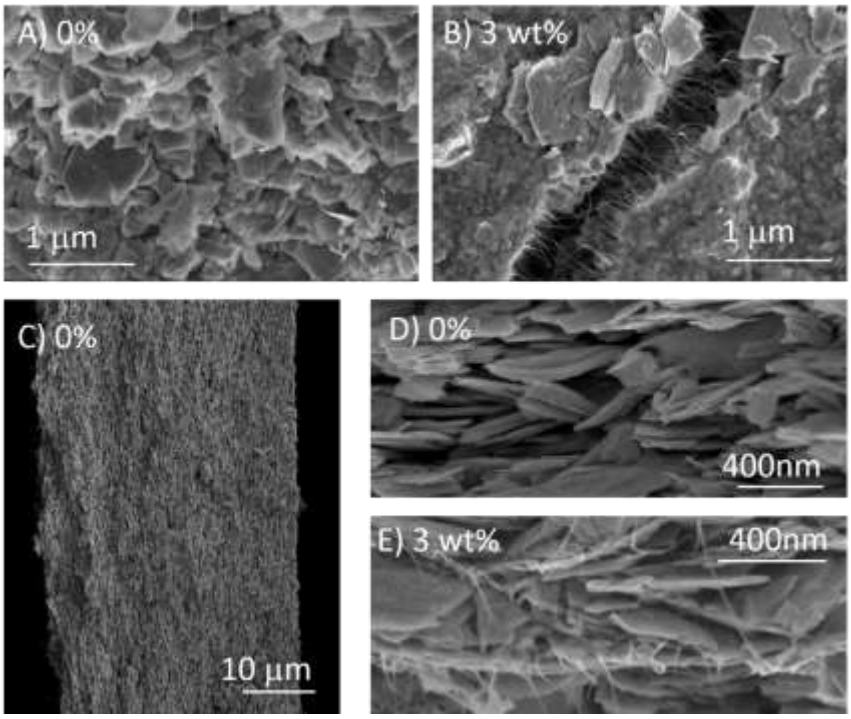

Figure 2: Initial SEM characterisation of networks. (A-B) Images of the surface of an MoS_2-only film (A) and a 3 wt% SWNT:MoS_2 composite film (B). (C) Low magnification image of the cross section of an MoS_2-only film. (D-E) High magnification images of fracture surfaces of an MoS_2-only film (D) and a 3 wt% SWNT:MoS_2 composite film (E).

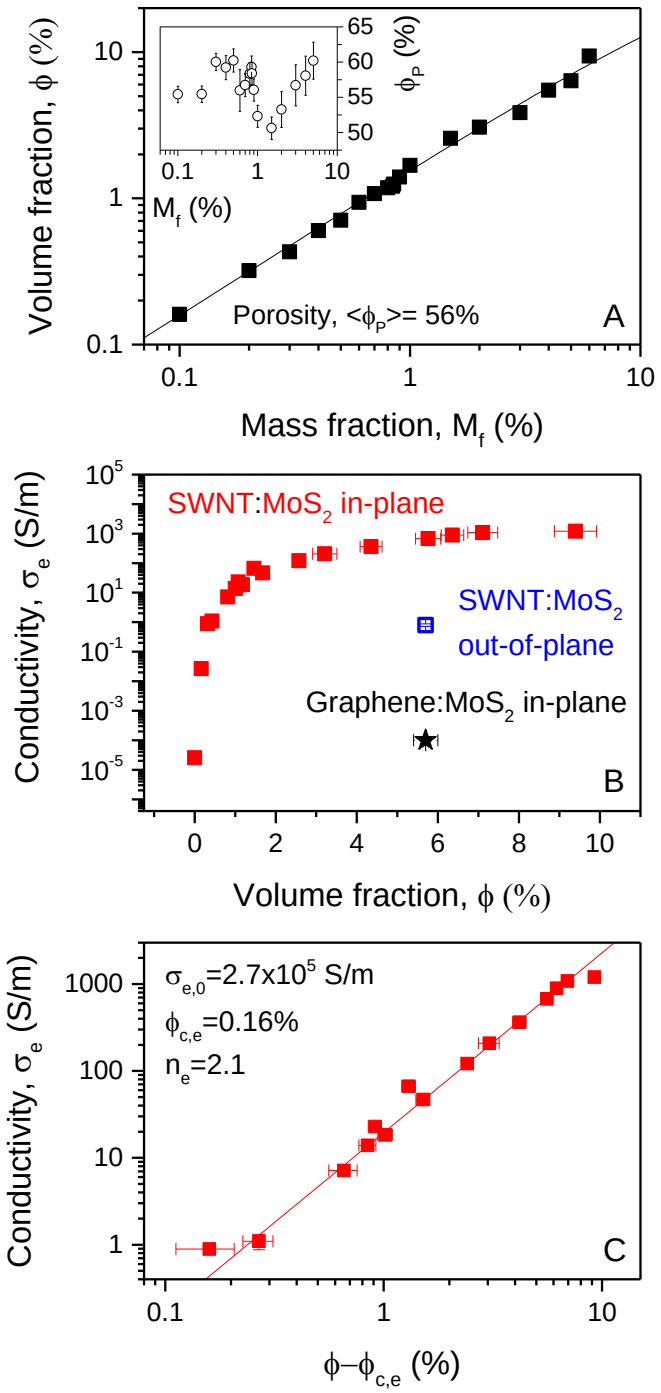

Figure 3: Structural and electrical characterisation of SWNT:MoS_2 composite films. (A) Composite film volume fraction plotted versus mass fraction. The line is a fit to equation 1 which yields a mean film porosity of 56%. Inset: Film porosity (calculated using equation 1) plotted versus nanotube mass fraction. (B) Composite in-plane conductivity versus SWNT volume fraction. Also shown are the out of plane conductivity as well as the in-plane conductivity for a Graphene:MoS_2 composite film. (C) Percolation plot with a fit to equation 2 and the percolation parameters given in the panel.

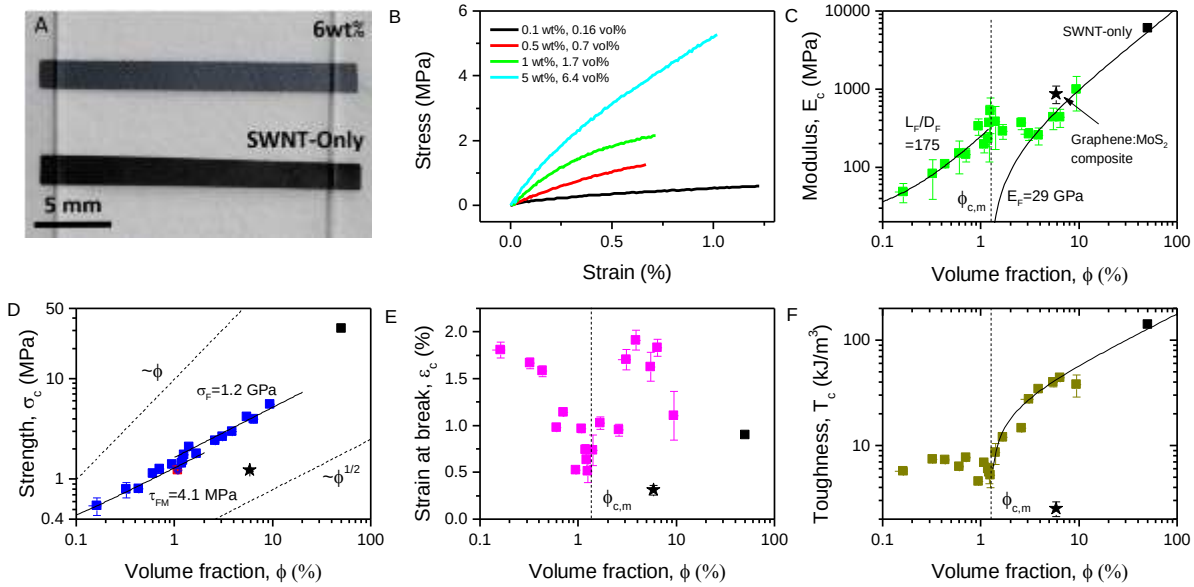

Figure 4: Tensile mechanical properties of SWNT:MoS_2 composite films. (A) Photograph of a 6 wt% SWNT:MoS_2 composite strip and a SWNT-only strip, similar to those used for tensile testing. (B) Subset of representative stress-strain curves for composite films of various nanotube loadings. (C-F) Plots of the composite modulus, strength, strain-at-break and tensile toughness (work done per unit volume at fracture, calculated from the area under the stress-strain curves) as a function of nanotube volume fraction. The black stars represent data points for an Graphene:MoS_2 composite. The black squares represent a SWNT-only film (~25 μm thick) that had a nanotube volume fraction of ~50% due to its porosity. In (C) black lines represent fits to equations 4 and 5 respectively. In (D), the solid lines represent fits to equations 6c and 6d while the dashed lines represent linearity and square root scaling behaviour. In (F), the data have been fitted to equation 7f. In C, E and F, the vertical dashed lines represent the mechanical percolation threshold, $\phi_{c,m}$.

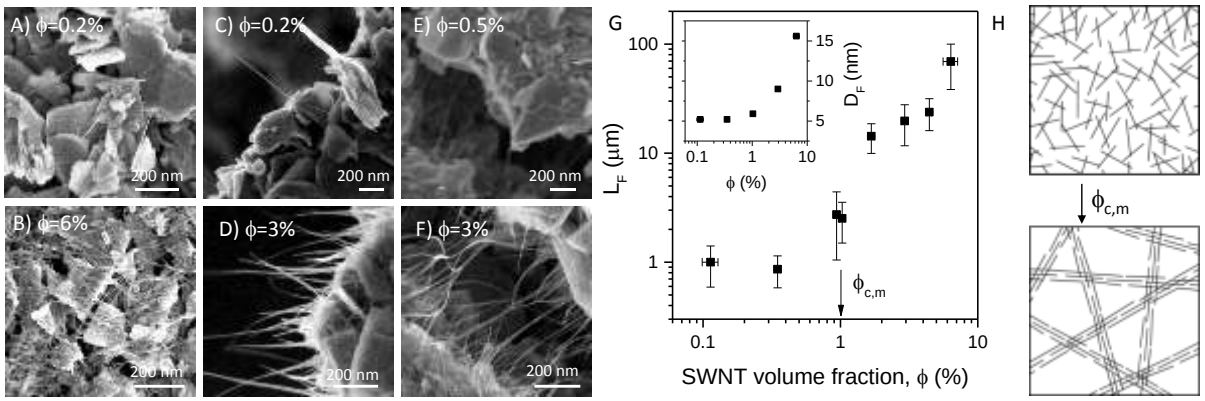

Figure 5: Nanotube network structure. (A-F) SEM images of the 1D:2D nano:nano composites with SWNT volume fractions below (top row, A, C, E) and above (bottom row, B, D, F) 1 vol%. The SEM images show planar surfaces (A-B), fracture surfaces (C-D) and surface cracks (E-F). There is a clear transition from isolated SWNTs (or very thin bundles) at low volume fraction to a network of ropes at higher loadings. (G) SWNT bundle/rope length as a function of SWNT volume fraction. The mechanical percolation threshold is indicated approximately by the arrow. Inset: Bundle/Rope diameter as a function of SWNT volume fraction. (H) Schematic showing the proposed network morphologies. At low-ϕ, the nanotube network consists of a sparse network of individual bundles loosely interconnected. In this arrangement the bundles maintain some of their individual character. However, at high-ϕ, almost all nanotubes have formed into extremely long ropes, almost all of which belong to the overall nanotube network. Individual bundles do not exist and ends are rarely seen unless the material is fractured. This transition happens at the mechanical percolation threshold, $\phi_{c,m}$, which we propose occurs around 1 vol%.

References

1. Zhang, Q.; Huang, J. Q.; Qian, W. Z.; Zhang, Y. Y.; Wei, F., The Road for Nanomaterials Industry: A Review of Carbon Nanotube Production, Post-Treatment, and Bulk Applications for Composites and Energy Storage. *Small* **2013,** 9, 1237-1265.
2. Wang, W.; Ciselli, P.; Kuznetsov, E.; Peijs, T.; Barber, A. H., Effective Reinforcement in Carbon Nanotube - Polymer Composites. *Philosophical Transactions of the Royal Society a-Mathematical Physical and Engineering Sciences* **2008,** 366, 1613-1626.
3. Huang, X.; Qi, X. Y.; Boey, F.; Zhang, H., Graphene-Based Composites. *Chem. Soc. Rev.* **2012,** 41, 666-686.
4. Young, R. J.; Kinloch, I. A.; Gong, L.; Novoselov, K. S., The Mechanics of Graphene Nanocomposites: A Review. *Compos. Sci. Technol.* **2012,** 72, 1459-1476.

5. Hull, D.; Clyne, T. W., *An Introduction to Composite Materials*. Cambridge University Press: 1996.
6. Khan, U.; O'Connor, I.; Gun'ko, Y. K.; Coleman, J. N., The Preparation of Hybrid Films of Carbon Nanotubes and Nano-Graphite/Graphene with Excellent Mechanical and Electrical Properties. *Carbon* **2010,** 48, 2825-2830.
7. Lota, G.; Fic, K.; Frackowiak, E., Carbon Nanotubes and Their Composites in Electrochemical Applications. *Energy Environ. Sci.* **2011,** 4, 1592-1605.
8. Zhou, M.; Li, X. L.; Wang, B.; Zhang, Y. B.; Ning, J.; Xiao, Z. C.; Zhang, X. H.; Chang, Y. H.; Zhi, L. J., High-Performance Silicon Battery Anodes Enabled by Engineering Graphene Assemblies. *Nano Lett.* **2015,** 15, 6222-6228.
9. Zhu, X. J.; Hu, J.; Dai, H. L.; Ding, L.; Jiang, L., Reduced Graphene Oxide and Nanosheet-Based Nickel Oxide Microsphere Composite as an Anode Material for Lithium Ion Battery. *Electrochim. Acta* **2012,** 64, 23-28.
10. Chang, K.; Chen, W. X., L-Cysteine-Assisted Synthesis of Layered Mos2/Graphene Composites with Excellent Electrochemical Performances for Lithium Ion Batteries. *ACS Nano* **2011,** 5, 4720-4728.
11. David, L.; Bhandavat, R.; Singh, G., Mos2/Graphene Composite Paper for Sodium-Ion Battery Electrodes. *ACS Nano* **2014,** 8, 1759-1770.
12. Liu, H. M.; Yang, W. S., Ultralong Single Crystalline V2o5 Nanowire/Graphene Composite Fabricated by a Facile Green Approach and Its Lithium Storage Behavior. *Energy Environ. Sci.* **2011,** 4, 4000-4008.
13. Zhang, S.; Zhu, L. X.; Song, H. H.; Chen, X. H.; Zhou, J. S., Enhanced Electrochemical Performance of Mno Nanowire/Graphene Composite During Cycling as the Anode Material for Lithium-Ion Batteries. *Nano Energy* **2014,** 10, 172-180.
14. Liu, Y. P.; He, X. Y.; Hanlon, D.; Harvey, A.; Khan, U.; Li, Y. G.; Coleman, J. N., Electrical, Mechanical, and Capacity Percolation Leads to High-Performance Mos2/Nanotube Composite Lithium Ion Battery Electrodes. *ACS Nano* **2016,** 10, 5980-5990.
15. Wang, D. N.; Li, X. F.; Yang, J. L.; Wang, J. J.; Geng, D. S.; Li, R. Y.; Cai, M.; Sham, T. K.; Sun, X. L., Hierarchical Nanostructured Core-Shell Sn@C Nanoparticles Embedded in Graphene Nanosheets: Spectroscopic View and Their Application in Lithium Ion Batteries. *Phys. Chem. Chem. Phys.* **2013,** 15, 3535-3542.
16. Zhou, J. S.; Ma, L. L.; Song, H. H.; Wu, B.; Chen, X. H., Durable High-Rate Performance of Cuo Hollow Nanoparticles/Graphene-Nanosheet Composite Anode Material for Lithium-Ion Batteries. *Electrochem. Commun.* **2011,** 13, 1357-1360.
17. DiLeo, R. A.; Frisco, S.; Ganter, M. J.; Rogers, R. E.; Raffaelle, R. P.; Landi, B. J., Hybrid Germanium Nanoparticle-Single-Wall Carbon Nanotube Free-Standing Anodes for Lithium Ion Batteries. *J. Phys. Chem. C* **2011,** 115, 22609-22614.
18. Kwak, W. J.; Lau, K. C.; Shin, C. D.; Amine, K.; Curtiss, L. A.; Sun, Y. K., A Mo2c/Carbon Nanotube Composite Cathode for Lithium-Oxygen Batteries with High Energy Efficiency and Long Cycle Life. *ACS Nano* **2015,** 9, 4129-4137.
19. Zhu, C. B.; Mu, X. K.; van Aken, P. A.; Maier, J.; Yu, Y., Fast Li Storage in Mos2-Graphene-Carbon Nanotube Nanocomposites: Advantageous Functional Integration of 0d, 1d, and 2d Nanostructures. *Adv. Energy Mater.* **2015,** 5.
20. Higgins, T. M.; McAteer, D.; Coelho, J. C. M.; Sanchez, B. M.; Gholamvand, Z.; Moriarty, G.; McEvoy, N.; Berner, N. C.; Duesberg, G. S.; Nicolosi, V.; Coleman, J. N., Effect of Percolation on the Capacitance of Supercapacitor Electrodes Prepared from Composites of Manganese Dioxide Nanoplatelets and Carbon Nanotubes. *ACS Nano* **2014,** 8, 9567-9579.
21. Li, L.; Hu, Z. A.; An, N.; Yang, Y. Y.; Li, Z. M.; Wu, H. Y., Facile Synthesis of Mno2/Cnts Composite for Supercapacitor Electrodes with Long Cycle Stability. *J. Phys. Chem. C* **2014,** 118, 22865-22872.
22. Peng, S. J.; Li, L. L.; Han, X. P.; Sun, W. P.; Srinivasan, M.; Mhaisalkar, S. G.; Cheng, F. Y.; Yan, Q. Y.; Chen, J.; Ramakrishna, S., Cobalt Sulfide Nanosheet/Graphene/Carbon Nanotube Nanocomposites as Flexible Electrodes for Hydrogen Evolution. *Angew. Chem.,Int. Ed.* **2014,** 53, 12594-12599.

23. McAteer, D.; Gholamvand, Z.; McEvoy, N.; Harvey, A.; O'Malley, E.; Duesberg, G. S.; Coleman, J. N., Thickness Dependence and Percolation Scaling of Hydrogen Production Rate in Mos2 Nanosheet and Nanosheet-Carbon Nanotube Composite Catalytic Electrodes. *ACS Nano* **2016,** 10, 672-683.
24. Cao, X. H.; Tan, C. L.; Zhang, X.; Zhao, W.; Zhang, H., Solution-Processed Two-Dimensional Metal Dichalcogenide-Based Nanomaterials for Energy Storage and Conversion. *Adv. Mater.* **2016,** 28, 6167-6196.
25. Zhao, M. Q.; Zhang, Q.; Huang, J. Q.; Wei, F., Hierarchical Nanocomposites Derived from Nanocarbons and Layered Double Hydroxides - Properties, Synthesis, and Applications. *Adv. Funct. Mater.* **2012,** 22, 675-694.
26. Singh, K. B.; Tirumkudulu, M. S., Cracking in Drying Colloidal Films. *Phys. Rev. Lett.* **2007,** 98.
27. McAteer, D.; Godwin, I. J.; Ling, Z.; Harvey, A.; He, L.; Boland, C. S.; Vega-Mayoral, V.; Szydłowska, B.; Rovetta, A. A.; Backes, C.; Boland, J. B.; Chen, X.; Lyons, M. E. G.; Coleman, J. N., Liquid Exfoliated Co(Oh)2 Nanosheets as Low-Cost, yet High-Performance, Catalysts for the Oxygen Evolution Reaction. *Adv. Energy Mater.*, 1702965-n/a.
28. Xiong, Z.; Yun, Y. S.; Jin, H. J., Applications of Carbon Nanotubes for Lithium Ion Battery Anodes. *Materials* **2013,** 6, 1138-1158.
29. Chhowalla, M.; Shin, H. S.; Eda, G.; Li, L. J.; Loh, K. P.; Zhang, H., The Chemistry of Two-Dimensional Layered Transition Metal Dichalcogenide Nanosheets. *Nature Chem.* **2013,** 5, 263-275.
30. Bonaccorso, F.; Bartolotta, A.; Coleman, J. N.; Backes, C., 2d-Crystal-Based Functional Inks. *Adv. Mater.* **2016,** 28, 6136-6166.
31. Coleman, J. N.; Lotya, M.; O'Neill, A.; Bergin, S. D.; King, P. J.; Khan, U.; Young, K.; Gaucher, A.; De, S.; Smith, R. J.; Shvets, I. V.; Arora, S. K.; Stanton, G.; Kim, H. Y.; Lee, K.; Kim, G. T.; Duesberg, G. S.; Hallam, T.; Boland, J. J.; Wang, J. J.; Donegan, J. F.; Grunlan, J. C.; Moriarty, G.; Shmeliov, A.; Nicholls, R. J.; Perkins, J. M.; Grieveson, E. M.; Theuwissen, K.; McComb, D. W.; Nellist, P. D.; Nicolosi, V., Two-Dimensional Nanosheets Produced by Liquid Exfoliation of Layered Materials. *Science* **2011,** 331, 568-571.
32. Cunningham, G.; Lotya, M.; McEvoy, N.; Duesberg, G. S.; van der Schoot, P.; Coleman, J. N., Percolation Scaling in Composites of Exfoliated Mos2 Filled with Nanotubes and Graphene. *Nanoscale* **2012,** 4, 6260-6264.
33. Ajayan, P. M.; Schadler, L. S.; Giannaris, C.; Rubio, A., Single-Walled Carbon Nanotube–Polymer Composites: Strength and Weakness. *Adv. Mater.* **2000,** 12, 750-753.
34. Kelly, A. G.; Hallam, T.; Backes, C.; Harvey, A.; Esmaeily, A. S.; Godwin, I.; Coelho, J.; Nicolosi, V.; Lauth, J.; Kulkarni, A.; Kinge, S.; Siebbeles, L. D. A.; Duesberg, G. S.; Coleman, J. N., All-Printed Thin-Film Transistors from Networks of Liquid-Exfoliated Nanosheets. *Science* **2017,** 356, 69-72.
35. Blighe, F. M.; Lyons, P. E.; De, S.; Blau, W. J.; Coleman, J. N., On the Factors Controlling the Mechanical Properties of Nanotube Films. *Carbon* **2008,** 46, 41-47.
36. Ling, Z.; Harvey, A.; McAteer, D.; Godwin, I. J.; Szydłowska, B.; Griffin, A.; Vega, V.; Song, Y.; Seral-Ascaso, A.; Nicolosi, V.; Coleman, J., Quantifying the Role of Nanotubes in Nano:Nano Composite Supercapacitor Electrodes. *Adv. Energy Mater.*, 1702364-n/a.
37. Stauffer, D.; Aharony, A., *Introduction to Percolation Theory*. CRC Press: 1994.
38. Bauhofer, W.; Kovacs, J. Z., A Review and Analysis of Electrical Percolation in Carbon Nanotube Polymer Composites. *Compos. Sci. Technol.* **2009,** 69, 1486-1498.
39. Balberg, I., Limits on the Continuum-Percolation Transport Exponents. *Phys. Rev. B* **1998,** 57, 13351-13354.
40. Johner, N.; Grimaldi, C.; Balberg, I.; Ryser, P., Transport Exponent in a Three-Dimensional Continuum Tunneling-Percolation Model. *Phys. Rev. B* **2008,** 77.
41. Coleman, J. N.; Khan, U.; Blau, W. J.; Gun'ko, Y. K., Small but Strong: A Review of the Mechanical Properties of Carbon Nanotube-Polymer Composites. *Carbon* **2006,** 44, 1624-1652.
42. Giordani, S.; Bergin, S. D.; Nicolosi, V.; Lebedkin, S.; Kappes, M. M.; Blau, W. J.; Coleman, J. N., Debundling of Single-Walled Nanotubes by Dilution: Observation of Large Populations of Individual Nanotubes in Amide Solvent Dispersions. *J. Phys. Chem. B* **2006,** 110, 15708-15718.

43. van Hecke, M., Jamming of Soft Particles: Geometry, Mechanics, Scaling and Isostaticity. *Journal of Physics-Condensed Matter* **2010,** 22.
44. Song, Y. I.; Lee, J. W.; Kim, T. Y.; Jung, H. J.; Jung, Y. C.; Suh, S. J.; Yang, C.-M., Performance-Determining Factors in Flexible Transparent Conducting Single-Wall Carbon Nanotube Film. *Carbon Letters* **2013,** 14, 255-258.
45. Young, R. J.; Liu, M.; Kinloch, I. A.; Li, S.; Zhao, X.; Vallés, C.; Papageorgiou, D. G., The Mechanics of Reinforcement of Polymers by Graphene Nanoplatelets. *Compos. Sci. Technol.* **2018,** 154, 110-116.
46. Rosenthal, J., A Model for Determining Fiber Reinforcement Efficiencies and Fiber Orientation in Polymer Composites. *Polym. Compos.* **1992,** 13, 462-466.
47. Cox, H. L., The Elasticity and Strength of Paper and Other Fibrous Materials. *British Journal of Applied Physics* **1952,** 3, 72-79.
48. Raisanen, V. I.; Alava, M. J.; Niskanen, K. J.; Nieminen, R. M., Does the Shear-Lag Model Apply to Random Fiber Networks? *J. Mater. Res.* **1997,** 12, 2725-2732.
49. Kis, A.; Csanyi, G.; Salvetat, J. P.; Lee, T. N.; Couteau, E.; Kulik, A. J.; Benoit, W.; Brugger, J.; Forro, L., Reinforcement of Single-Walled Carbon Nanotube Bundles by Intertube Bridging. *Nat. Mater.* **2004,** 3, 153-157.
50. Sampson, W. W., Materials Properties of Paper as Influenced by Its Fibrous Architecture. *Int. Mater. Rev.* **2009,** 54, 134-156.
51. Lees, J. K., A Study of the Tensile Strength of Short Fiber Reinforced Plastics. *Polym. Eng. Sci.* **1968,** 8, 195-201.
52. Chen, P. E., Strength Properties of Discontinuous Fiber Composites. *Polym. Eng. Sci.* **1971,** 11, 51-56.
53. Gibson, R. F., *Principles of Composite Material Mechanics, Second Edition*. CRC Press: 2007.
54. Li, F.; Cheng, H. M.; Bai, S.; Su, G.; Dresselhaus, M. S., Tensile Strength of Single-Walled Carbon Nanotubes Directly Measured from Their Macroscopic Ropes. *Appl. Phys. Lett.* **2000,** 77, 3161-3163.
55. Xiao, T.; Ren, Y.; Liao, K.; Wu, P.; Li, F.; Cheng, H. M., Determination of Tensile Strength Distribution of Nanotubes from Testing of Nanotube Bundles. *Compos. Sci. Technol.* **2008,** 68, 2937-2942.
56. Tsuda, T.; Ogasawara, T.; Deng, F.; Takeda, N., Direct Measurements of Interfacial Shear Strength of Multi-Walled Carbon Nanotube/Peek Composite Using a Nano-Pullout Method. *Compos. Sci. Technol.* **2011,** 71, 1295-1300.
57. Nie, M.; Kalyon, D. M.; Pochiraju, K.; Fisher, F. T., A Controllable Way to Measure the Interfacial Strength between Carbon Nanotube and Polymer Using a Nanobridge Structure. *Carbon* **2017,** 116, 510-517.
58. Barber, A. H.; Cohen, S. R.; Wagner, H. D., Measurement of Carbon Nanotube-Polymer Interfacial Strength. *Appl. Phys. Lett.* **2003,** 82, 4140-4142.
59. Vilatela, J. J.; Elliott, J. A.; Windle, A. H., A Model for the Strength of Yarn-Like Carbon Nanotube Fibers. *Acs Nano* **2011,** 5, 1921-1927.
60. Khan, U.; May, P.; O'Neill, A.; Vilatela, J. J.; Windle, A. H.; Coleman, J. N., Tuning the Mechanical Properties of Composites from Elastomeric to Rigid Thermoplastic by Controlled Addition of Carbon Nanotubes. *Small* **2011,** 7, 1579-1586.
61. Malmberg, B., Relationships between Properties of Laboratory Handsheets Pressed with Different Wet Pressures. *Svensk Papperstidning-Nordisk Cellulosa* **1970,** 73, 334-&.
62. Seth, R. S.; Page, D. H., The Stress-Strain Curve of Paper. In *VIIth Fund. Res. Symp.*, Brander, J., Ed. Cambridge, 1981.
63. Wagner, H. D.; Ajayan, P. M.; Schulte, K., Nanocomposite Toughness from a Pull-out Mechanism. *Compos. Sci. Technol.* **2013,** 83, 27-31.